Preparation and Electrochemical Corrosion Behavior of Bulk Nanocrystalline Ingot Iron in HCl Acid Solution

S. G. Wang,*,† C. B. Shen,‡,§ K. Long,‡ H. Y. Yang,‡ F. H. Wang,‡ and Z. D. Zhang†

Shenyang National Laboratory for Materials Sciences, Institute of Metal Research and International Centre for Materials Physics, Chinese Academy Sciences, 72 Wenhua Road, 110016, Shenyang, P. R. China; State Key Laboratory for Corrosion and Protection, Institute of Metal Research, Chinese Academy Sciences, 62 Wencui Road, 110016, Shenyang, P. R. China; and Department of Materials Science and Engineering, Dalian Jiaotong University, 793 Huanghe Road, 116028, Dalian, P. R. China

Received: August 17, 2004; In Final Form: November 15, 2004

Bulk nanocrystalline ingot iron (BNII) was produced by the severe rolling technique. The corrosion behaviors of BNII and as-received conventional polycrystalline ingot iron (CPII) in 1 M HCl solution were investigated by potentiodynamic polarization tests, electrochemical impedance spectroscopy measurement, and immersion tests at room temperature. For BNII, the anodic dissolution process is inhibited, but the cathodic process is enhanced. The corrosion current and average corrosion rate of BNII are 0.479 and 0.391 those of CPII, respectively. The resistance of the charge transfer of BNII is about 1.59 times higher than that of CPII. These results indicate that the corrosion resistance of BNII is improved in comparison with CPII.

I. Introduction

Nanocrystalline materials have been the focus of much attention since their first introduction over two decades ago.[1] However, because of the metastable nature of these microstructures, nanostructured grain materials were difficult to produce in bulk form and were usually produced by special preparation techniques. Recently, various techniques (e.g., electrodeposition,[2] vapor condensation,[3] ball milling,[4] etc.) have been developed to produce many nanomaterials. There is a considerable interest in the nonpowder metallurgical technique because the problem of residual porosity can be completely avoided.[5,6] However, there is more considerable interest in the technique for larger dimension bulk nanostructured materials because a larger dimension of specimen can meet more requirements for different experiments and could be potential to be applied in industry. Materials with nanostructured gain microstructure exhibit improved mechanical and other properties over their coarse-grained counterpart.[1] The electrochemical corrosion property has received only limited attention. This makes it difficult to predict the electrochemical behavior of these materials from their coarse-grained and amorphous analogues. It has been recognized that grain boundaries play a primary role in many properties of ultrafine-grained (UFG) materials.[5] The nanocrystalline alloy $Fe_{32}Ni_{36}Cr_{14}P_{12}B_6$ produced by annealing the melt-spun amorphous ribbon had better corrosion resistance than its amorphous counterpart.[7] This was explained in terms of Cr enrichment at the specimen surface due to more rapid grain boundary diffusion paths. However, the corrosion rate of the nanocrystallized surface of low carbon steel fabricated using ultrasonic shot peening was higher than that of its low carbon steel surface counterpart.[8] The significant degradation of corrosion resistance was also reported for nanocrystalline Ni−P with grain sizes of 8.4 and 22.6 nm.[9] Moreover, the anticorrosion properties of nanocrystalline Ni were shown to display the same active−passive−transpassive behavior exhibited by conventional Ni in H_2SO_4 solution.[10] The corrosion behavior of UFG Cu produced by equal channel angular extrusion was investigated, which was no change compared with that of coarse-grained Cu.[11]

We describe the new processing technique for preparation of larger bulk nanocrystalline ingot iron. We call it as severe rolling. To the authors' knowledge, there have been no reports on electrochemical corrosion behavior of bulk nanocrystalline ingot iron (BNII). In this work, the electrochemical corrosion behaviors of BNII and conventional polycrystalline ingot iron (CPII) are investigated by the potentiodynamic polarization (PDP) test, immersion experiment, and electrochemical impedance spectroscopy (EIS) technique.

II. Experimental Section

Preparation and Characterization. CPII is a 40 × 800 mm rod. The details of this processing technique are as follows: (1) CPII was annealed to obtain single phase Austenite structure at 924 °C for 2 h and was rolled as 800 × 100 × 15 mm sheets. This process is called control rolling at austenite recrystallization; it is also called mode I control rolling. (2) The CPII sheets obtained in (1) were rolled as 800 × 100 × 5 mm sheets for eight passes from 924 °C to Ar_3 temperature. The deformation is about 67% in this process. This process is called rolling at austenite nonrecrystallization phase and is also called mode II control rolling. (3) The iron sheets obtained in (2) were rolled as 800 × 100 × 1.0−1.2 mm iron sheets for 14 passes from Ar_3 temperature to 220 °C, and then rolled iron sheets were cooled to room temperature. The deformation is about 76% in this process. This process is called rolling in two phases,

† Institute of Metal Research and International Centre for Materials Physics, Chinese Academy Sciences.
‡ Institute of Metal Research, Chinese Academy Sciences.
§ Dalian Jiaotong University.
* Address correspondence to this author: Fax 86-24-23891320; e-mail sgwang@imr.ac.cn.

10.1021/jp046297v CCC: $30.25
Published on Web 01/20/2005

($\gamma + \alpha$) and α phase, and is also called mode III control rolling and rolling in α phase. The total deformation in the three processes is about 93%. We could prepare bulk nanocrystalline ingot iron (BNII) by the three processes. The microstructure of BNII was examined with a Philips CM200 transmission electron microscope (TEM) operated at 200 kV and X-ray diffraction (XRD). The microstructure of CPII was examined with XRD and optical microscopy. The TEM specimens of BNII were provided for the investigation of grain orientations by the electron backscattering diffraction (EBSD) method in JEOL-JSM-6301F scanning electron microscope operated at 15 kV.

Electrochemical Experiments. All the specimens in this study were from the third step of severe rolling without any heat treatments. Electrochemical and immersion tests were performed in 1 M HCl solution at ambient temperature. The solution was deaerated with high-purity nitrogen during the whole experimental process. The tested surface in all experiments was the rolled surface.

Potentiodynamic polarization tests were carried out using a PARC Parstat 2263 system equipped with POWERCORR software. The electrochemical cell was a classical three-electrode system. The reference electrode was a saturated calomel electrode (SCE), and the counter electrode was a Pt plate. The potential was scanned from 400 to -300 mV for BNII and 300 to -200 mV for CPII vs the open-circuit potential (E_{ocp}) of BNII and CPII, respectively. Scan speed was set at 0.166 mV/s. Working area was 1 cm^2. The working electrode was first wet-abraded successively by emery paper up to 1000# SiC and then electropolished. Finally, the working surface was washed with double-distilled water, degreased with acetone, and dried with hot hair. These treatments ensured good reproducibility of electrochemical measurements. Prior to PDP test, all specimens were cathodically polarized at a potential of -350 mV vs a saturated calomel electrode (SCE) for 15 min to remove any surface films. The applied potential was then removed, and the system was monitored until a steady-state open-circuit potential E_{ocp} was reached. Corrosion current (I_{corr}), anodic Tafel slope (B_a), and cathodic Tafel slope (B_c) were provided after analysis by the POWERCORR software.

Immersion tests were carried out in a glass flask with a volume of 600 mL. The samples were also treated the same as in PDP test. The samples were suspended at the bottom of the flask. They were washed with double-distilled water and acetone after 6 h exposure and then were dried and weighed. No extra process was needed for getting rid of the residual sticking to the sample because of the solubility of ferric chloride. The morphologies of corrosion surfaces were observed by SEM.

EIS measurement was carried out with the EG&G PARC Parstat 2263 controlled by POWERSINE at E_{ocp} and used an AC sine wave amplitude of 10 mV. The applied frequency ranged from 10^5 to 10^{-2} Hz. The samples for this experiment were also treated the same as in PDP test. The impedance data, R_s, the resistance of solution, R_t, the resistance of charge transfer, and C_{dl}, the double-layer capacity of the interface, were analyzed by Zsimpwin software. The Nyquist plots of BNII and CPII were drawn.

III. Results of Microstructure and Electrochemical Properties

XRD, Optical Microscopy, TEM, and EBSD Results. Figure 1 represents XRD results for BNII and CPII. The XRD peaks of BNII are broadened, indicating a grain refinement. The peaks of BNII are higher than those of CPII, which results from the textured structure in BNII. The grain size near the surface of the BNII is about 38.9 nm as measured by XRD. The grain size of CPII is about 50 μm, as shown in Figure 2a. The BNII microstructure investigated by TEM is shown in Figure 2b. It is clear from Figure 2b that the grain size of BNII varies from 50 to 89 nm with an equiaxed structure, and the structure is nearly isotropic. The difference data for the grain size, obtained by XRD and TEM, result from the fact that the grain size near the surface is smaller than that in the middle section after severe rolling. The distribution of misorientation angles for BNII grain boundaries is shown as Figure 3 obtained by EBSD measurement; the mean misorientation angle of BNII grain boundaries is 27.4°. From Figure 3, the total of relative frequency of misorientation angles larger than 15° is about 82%, which demonstrates that most of BNII grain boundaries are high-angle boundaries whose misorientation angles are larger than 15°. The selected area diffraction pattern taken from the rolling plane are ringlike as shown in Figure 2b, which indicates that a number of different orientations can exist within the selected small area.

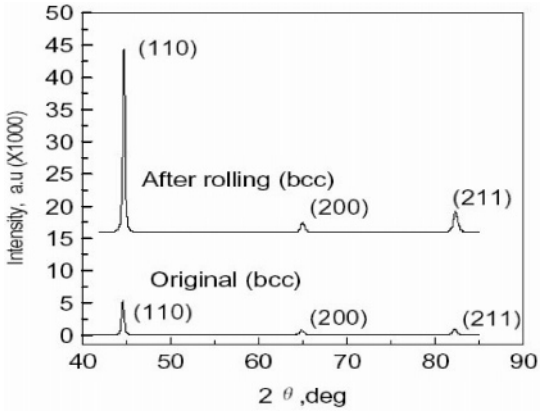

Figure 1. XRD patterns of BNII (after rolling) and CPII (original).

Immersion Tests and the Morphologies of Corrosion Surface for BNII and CPII. Immersion tests of ingot iron in HCl solution can be reliable for the determination of its average corrosion rate because the corrosion process of ingot iron is active dissolution. All data for immersion tests are listed in Table 1. m_1 and m_2 are the sample mass before and after corrosion, respectively, s is the area exposed in solution, t is the time of corrosion, v is corrosion rate of each measurement, and $\bar{v}$ is average corrosion rate.

$$v = \frac{m_1 - m_2}{st} \quad \text{and} \quad \bar{v} = \frac{\sum_{i=1}^{i=3} v_i}{3} \tag{1}$$

According to eq 1, $\bar{v}$ of BNII and CPII are 0.127×10^{-3} kg and 0.325×10^{-3} kg/(m^2 h), respectively. This result demonstrates that the corrosion resistance of BNII is improved, in comparison with that of CPII. After immersion tests, considerable difference between their corrosion morphologies was observed by SEM. As shown in Figure 4a, there is no such localized attack in anodic dissolution corrosion of BNII. This can be considered as a certain advantage of BNII for corrosion fatigue in hydrochloric acid solution. However, Figure 4b shows the localized attack suffered from Cl^- for CPII. The localized attack of CPII is supposed to result from the microcells formed around the carbon impurity, as shown in Figure 2a.

PDP Tests of BNII and CPII. PDP curves of BNII and CPII are shown in Figure 5. The electrochemical parameters B_a, B_c,

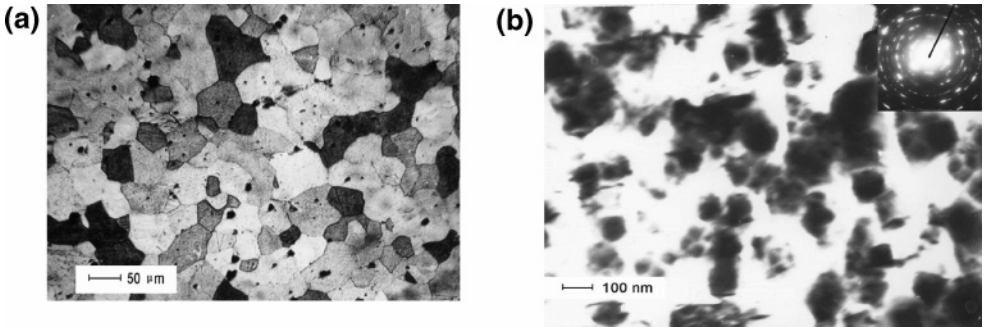

Figure 2. Metallograph of CPII (a) and TEM images of BNII (b).

TABLE 1: Results of Immersion Tests in 1 M HCl Solution at Room Temperature for BNII and CPII

sample no.	$s \times 10^{-6}$ (mm^2)	$m_1 \times 10^{-3}$ (kg)	$m_2 \times 10^{-3}$ (kg)	t (h)	$v \times 10^{-3}$ (kg/(m^2 h))	$\bar{v} \times 10^{-3}$ (kg/(m^2 h))
1 (nano-)	409	1.2864	1.2834	60	0.122	
2 (nano-)	402	1.2042	1.2010	60	0.132	0.127
3 (nano-)	415	1.4211	1.4179	60	0.129	
4 (coarse)	464	2.7264	2.7174	60	0.323	
5 (coarse)	467	2.9159	2.8068	60	0.325	0.325
6 (coarse)	465	2.7689	2.7598	60	0.326	

TABLE 2: Electrochemical Parameters of BNII and CPII in 1 M HCl Solution at Room Temperature

sample	B_a (mV dec^{-1})	B_c (mV dec^{-1})	E_{ocp} (mV)	I_{corr} (μA cm^{-2})	R_s (ohm m^2)	C_{dl} (μF cm^{-2})	R_t (ohm m^2)
nano-	83.89	151.18	−324.26	21.16	13.77	30.65	365
coarse	88.23	151.73	−438.33	44.15	13.59	28.57	141

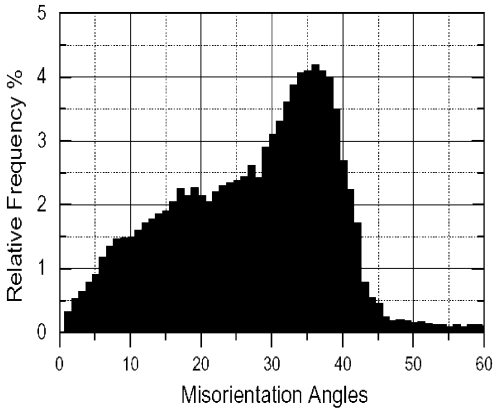

Figure 3. Distribution of misorientation angles for BNII grain boundaries observed from rolled plane.

E_{ocp}, and I_{corr} were obtained by fitting the curves with Powercorr software and are listed in Table 2. E_{ocp} of BNII is more positive than that of CPII. I_{corr} of BNII is only about half of CPII, indicating that the two materials are corroded at different rates. This result is consistent with that of immersion tests. As shown in Figure 5, BNII shows lower dissolution of anode rate than that of CPII and larger dissolution of cathode than that of CPII over the entire potential range. The reason for enhanced dissolution of cathode for BNII may result from refined carbon grains and microcell formed around carbon grains in BNII. Figure 5 and Table 2 indicate that the corrosion resistance of BNII in HCl solution is improved, in comparison with CPII. For UFG Cu,[11] Ni, and Ni-based alloys,[9,10] their PDP curves are the same as their counterparts. These differences may result from different preparation techniques.

EIS Measurement of BNII and CPII. The EIS spectra of BNII and CPII during 10 min immersion test are shown in Figure 6a. The circuit used for fitting the EIS data is a simplified Randles circuit, as shown in Figure 6b. The impedance of this circuit Z is composed of real (Z_{re}) and imaginary (Z_{im}) parts. It related to frequency of signal, the polarization resistance, the double-layer capacity of the interface, and the resistance of electrolyte.[12]

The fitted parameters R_s, R_t, and C_{dl} are shown in Table 2. R_t is inversely correlated to the corrosion rate. EIS measurement

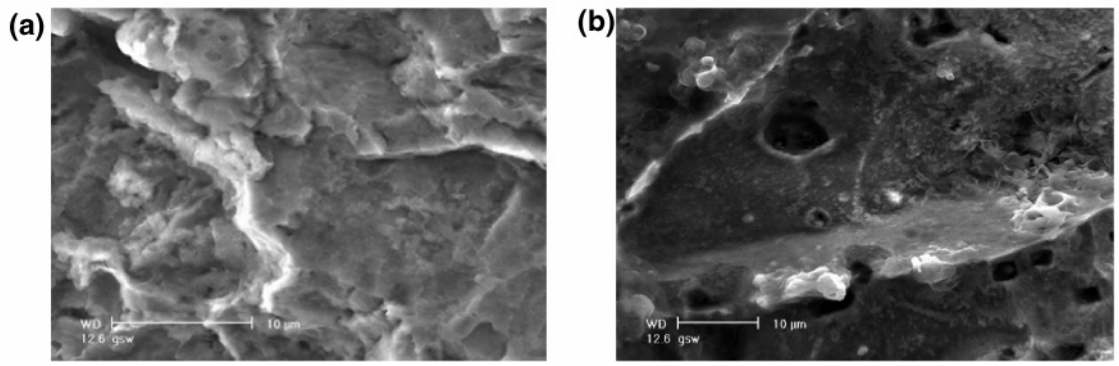

Figure 4. Corrosion surface morphologies of BNII and CPII: (a) for BNII; (b) for CPII.

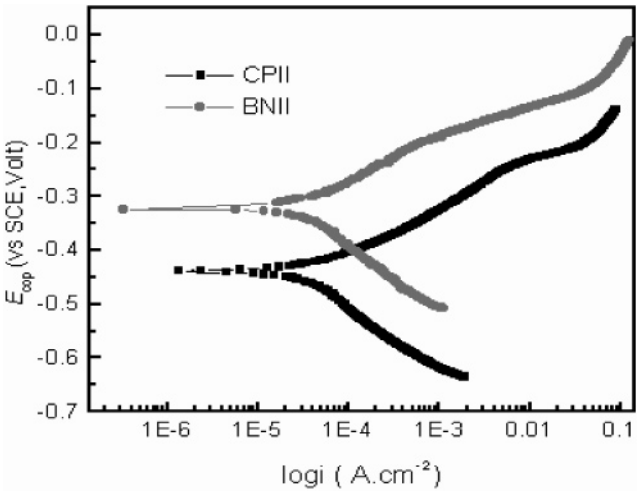

Figure 5. Potentiodynamic polarization curves of BNII and CPII.

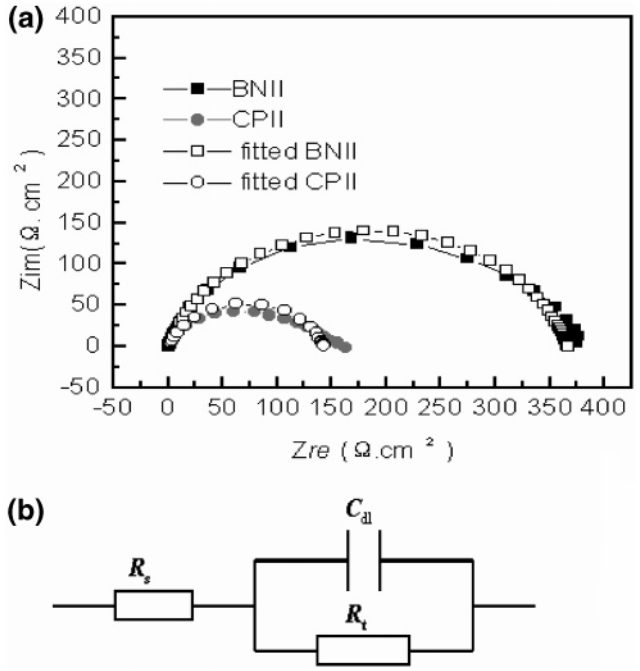

Figure 6. Nyquist plots of BNII and CPII (a) and equivalent circuit for each EIS spectrum (b).

indicates that the corrosion rate of BNII is lower than that of CPII. This result is consistent with the immersion tests and PDP tests. The Nyquist plot is composed of a single capacitance loop and a semicircle, which is attributed mainly to the transient resistance and the double-layer capacitance of the electrode. This also indicates that the charge-transfer process mainly controls the corrosion of iron.

IV. Discussion

It should be noted that the widths of rolled sheets were a constant (100 mm) in the second and third processes of the severe rolling technique. This can make to form the approximately equiaxed grains with high-angle boundaries. Ueji et al. have produced the equiaxed ultrafine grains with the mean diameter of 180 nm in plain low-carbon steel JIS-SS400 (0.13 wt % C; 0.01% Si; 0.37% Mn; 0.020% P; 0.0043% N) by simple cold rolling of 50% reduction in thickness and annealing of martensite starting structure.[13] So it is possible that we can produce more refined grains if the total deformation is larger than 50% in rolling processes for bcc structure materials.

The electrode reactions are known to be composed of the two partial reactions. The anodic reaction is

$$Fe_{(s)} \rightarrow Fe^{2+}_{(aq)} + 2e^- \tag{2}$$

and the cathodic partial reaction is

$$2H^+_{(aq)} + 2e^- \rightarrow H_{2(g)} \tag{3}$$

According to Faraday's law

$$\Delta W = \frac{A}{Fn} I_{corr} t \tag{4}$$

where ΔW is weight loss in immersion tests, A and n are atom weight (56 for iron) and chemical valence of iron (+2 in this study), respectively, F is Faraday constant (1 F = 96 494 coulombs), and I_{corr} of BNII and CPII are 12.2 and 31.2 μA/cm^2, respectively, from eq 4. According to the Stern−Geary equation

$$R_t = \frac{B_a B_c}{2.3(B_a + B_c)} \frac{1}{I_{corr}} \tag{5}$$

I_{corr} of BNII and CPII are 9.47 and 25.7 μA/cm^2. The results from the three tests above are identical within error, and the conclusions from these tests are in good agreement.

According to the PDP curve, I_{corr} of BNII is lower than that of CPII and E_{ocp} of BNII is more positive than that of CPII. R_t of BNII is larger than that of CPII. $\bar{v}$ of BNII is lower than that of CPII in immersion tests. These results show that CPII is more prone to corrosion than BNII. Although the cathodic reaction of BNII is enhanced, the anodic reaction of BNII is inhibited, and the inhibition effect exceeds the enhancement effect. It leads to reduction of the corrosion current density and inhibition of the overall corrosion. No localized attack is an advantage in engineering application for BNII. Superior localized corrosion resistance in HCl solution was observed for sputter-deposited nanocrystalline 304 stainless steel; the authors attributed it to the fine grain size and homogeneity of nanocrystalline metal.[15] The electroplated amorphous Ni−P did not passivate in H_2SO_4 solution.[16] In contrast, Diegle reported passivation for melt-spun amorphous Ni−P in the same solution.[14] This discrepancy might be due to the difference in preparation of materials. Grain size reduction had little effect on the overall corrosion performance of Co prepared by the electrodeposition technique.[18] The enhanced dissolution rates of nanocrystalline materials over their observed for conventional polycrystalline materials are due to the high volume fraction of grain boundaries and triple junction.[9,11] However, the two factors could not result from the enhanced dissolution rate of BNII over that of CPII. In fact, the corrosion properties of nanocrystalline materials depended strongly on the preparation technique, thermal history, material purity, and other factors.[5]

According to classical points of view, plastic deformation can result in degradation of corrosion resistance in hydrochloric acid.[19,20] The effects of plastic deformation are produced by an increase in the number and activity of surface site (emerging dislocation).[19] The increased corrosion rate of iron suffered from plastic deformation due to an increase in the rate of anodic dissolution; the hydrogen evolution reaction is only negligibly affected by plastic deformation.[20] For mechanically alloyed Co−Cu nanocrystalline, the corrosion rates are higher than those in as-cast alloys, which is attributed to high value of stored energy presented in mechanical alloying as a result of the severe plastic

deformation during ball milling.[21] It has been reported by Kirchheim that linear sweep voltamograms of pure nanocrystalline palladium obtained by a sputtering process presented a current density higher than that of pure microcrystalline. It is due to the poor consolidation of mechanically alloyed powder and/or the existence of high stored energy originated by the nanocrystalline grain size and the accumulation of the other crystal defects formed during the balling of the powder.[22] For BNII, high energy stores in it due to severe rolling. However, the results obtained in the present work are in contradiction to those of previous experiments. The main reason for enhanced corrosion properties of BNII in comparison with CPII may be related to the microstructure difference between them. For BNII, the preferential orientation is dominant, and the disordered orientation disappears, which can be obtained from Figure 1 where the peak of plane (110) of BNII is higher than that of CPII. The higher peak results from the textured structure after severe rolling. The surface of BNII becomes more compact and uniform than that of CPII. Another possible reason may be the existence of a reasonable degree of structural homogeneity and fine grain size on the surface after severe rolling[14,17] from Figure 2b. However, the reason for this needs to be investigated further.

V. Conclusions

The severe rolling technique can prepare bulk nancrystalline ingot iron, and it has potential to be industrialized. There is no localized attack for bulk nanocrystalline ingot iron produced by the severe rolling technique in 1 M HCl solution, which is a advantage in engineering application for BNII. The anodic dissolution process of BNII is inhibited, but the cathodic process is enhanced. The corrosion resistance of bulk nanocrystalline ingot iron has improved, in comparison with that of counterparts in 1 M HCl solution.

Acknowledgment. This project has been financially supported by the National Natural Science Foundation under Contract No. 10274087. S. G. Wang is extremely thankful to Professor Z. G. Wang for reviewing this manuscript.

References and Notes

(1) Gleiter, H. *Prog. Mater. Sci.* **1989**, *33*, 223.
(2) Erb, U.; El-Sherik, A. M.; Palumbo, G.; Aust, K. T. *Nanostruct. Mater.* **1993**, *2*, 383.
(3) Birringer, R.; Gleiter, H.; Klein, H. P.; Marquardt, P. *Phys. Lett. A* **1984**, *102*, 365.
(4) Koch, C. C. *Nanostruct Mater.* **1993**, *2*, 109.
(5) Valiev, R. Z.; Islamgaliev, R. K.; Alexandrov, I. V. *Prog. Mater. Sci.* **2000**, *45*, 103.
(6) Liu, Q.; Huang, X.; Lloyd, D. J.; Hansen, N. *Acta Mater.* **2002**, *50*, 3789.
(7) Thorpe, S. J.; Ramaswami, B.; Aust, K. T. *J. Eelctrochem. Soc.* **1988**, *135*, 2162.
(8) Li, Y.; Wang, F. H.; Liu, G. *J. Chin. Soc. Corros. Protect.* **2001**, *21*, 215.
(9) Rofagha, R.; Erb, U.; Ostrander, D.; Palumbo, G.; Aust, K. T. *Nanocryst. Mater.* **1993**, *2*, 1.
(10) Rofagha, R.; Langer, R.; Ei-Sherik, A. M.; Erb, U.; Palumbo, G.; Aust, K. T. *Scr. Metall.* **1991**, *25*, 2867.
(11) Vinogradov, A.; Mimaki, T.; Hashimoto, S.; Valiev, R. Z. *Scr. Mater.* **1999**, *41*, 319.
(12) Wu, X.; Ma, H.; Chen, S.; Xu, Z.; Sui, A. *J. Electrochem. Soc.* **1999**, *146*, 1847.
(13) Ueji, R.; Tsuji, N.; Minamino, Y.; Koizumi, Y. *Acta Mater.* **2002**, *50*, 4177.
(14) Diegle, R. B.; Clayton, C. R.; Lu, Y.; Sorensen, N. R. *J. Electrochem. Soc.* **1987**, *134*, 138.
(15) Inturi, R. B.; Szklarska-Smialowska, Z. *Corrosion* **1992**, *48*, 398.
(16) Carbajal, J. L.; White, R. E. *J. Electrochem. Soc.* **1988**, *135*, 2952.
(17) Kim, S. H.; Aust, K. T.; Erb, U.; Gonzalez, F.; Palumbo, G. *Scr. Mater.* **2003**, *48*, 1379.
(18) Pardo, A.; Otero, E.; Merino, M. C.; Lopez, M. D.; Vazquez, M.; Agudo, P. *Corros. Sci.* **2002**, *44*, 1193.
(19) Greene, N. D.; Saltzman, G. A. *Corrosion* **1964**, *29*, 293t.
(20) Foroulis, Z. A.; Uhlig, H. H. *J. Electrochem. Soc.* **1964**, *111*, 522.
(21) Lopez-Hirate, V. M.; Arce-Estrada, E. M. *Electrochim. Acta* **1997**, *42*, 61.
(22) Kirchheim, R.; Huang, X. Y.; Cui, P.; Birringer, R.; Gleiter, H. *Nanostuct. Mater.* **1992**, *1*, 167.